A dissertation

on

Synthesis and Characterization of $BaTiO_3$ by Co-Precipitation Method

submitted in partial fulfilment of

the requirement for the degree of

MASTER OF TECHNOLOGY

IN

NANOSCIENCE & TECHNOLOGY

by

PRANAV DHARMANI

Roll No. – 2K12/NST/014

Under the Supervision of

DR. AMRISH K. PANWAR

DEPARTMENT OF APPLIED PHYSICS

DELHI TECHNOLOGICAL UNIVERSITY

(FORMERLY DELHI COLLEGE OF ENGINEERING)

NEW DELHI-110042

2012-2014

CERTIFICATE

This is to certify that the dissertation entitled **"Synthesis and Characterization $BaTiO_3$ by Co-precipitation Method"** is being submitted by **Pranav Dharmani** bearing roll no. **2K12/NST/014** to the **Delhi Technological University, New Delhi,** for the degree of Master of Technology in **Nano Science and Technology**, run by Applied Physics Department is a bonafide work is carried out by him. The research work reported and the results presented in this thesis have not been submitted in parts or in full to any other University or Institute for the award of any degree or diploma.

Date: __/07/2014.

Dr. Amrish K. Panwar	**Prof. S. C. Sharma**
Supervisor	Head of Department
Department of Applied Physics	Department of Applied Physics
Delhi Technological University	Delhi Technological University
New Delhi, India	New Delhi, India

DECLARATION

I hereby declare that the work presented in this dissertation entitled **"Synthesis and Characterization $BaTiO_3$ by Co-precipitation Method"**, has been carried out by me under the guidance of **Dr. Amrish K. Panwar,** Assistant Professor and hereby submitted for the partial fulfillment for the award of degree of Master of Technology in Nanoscience and Technology at Applied Physics Department, Delhi Technological University (Formerly Delhi College of Engineering), New Delhi.

I further undertake that information and data enclosed in this dissertation is original and has not been submitted to any University/Institute for the award of any other degree.

Pranav Dharmani

2K12/NST/14

M.Tech. Nanoscience and Technology

Delhi Technological University

Delhi.

ACKNOWLEDGEMENTS

I wish to express my deep sense of gratitude to **Dr. Amrish K. Panwar**, Assistant Professor, Department of Applied Physics, Delhi Technological University, Delhi for introducing the present topic and for his inspiring guidance, constructive criticism and valuable suggestions throughout the project.

I would also like to express my indebtedness to **Dr. S.C. Sharma**, Head, Department of Applied Physics, Delhi Technological University, Delhi for providing all kinds of help required through the department.

I would to like to avail this opportunity also to acknowledge the scholarly inputs of **Dr. R.Bhattacharyya,** Adjunct Professor, IIEST, Shivpur, Howrah and formerly Sr. Scientist/Emeritus Scientist, NPL, New Delhi for his valuable who sharpened my critical abilities.

I would also like to thank to all my friends and colleagues who have patiently extended all sorts of help for accomplishing this work.

Above all, I am indebted to the Almighty for blessing me with potential to carry out the project besides my parents for encouraging me during the completion of the dissertation.

LIST OF FIGURES

LIST OF TABLES

LIST OF ABBREVIATIONS

AAG	Acetic Acid Gel
DPT	Diffused Phase Transition
DSC	Differential Scanning Calorimetry
MLCC	Multi Layer Ceramic Capacitor
nm	Nanometer
SEM	Scanning Electron Microscopy
SAG	Stearic Acid Gel
T_c	Curie Temperature
T.D.	Total Density
XRD	X Ray Diffraction

TABLE OF CONTENTS

ABSTRACT

Ferroelectric materials are key to many technologies due to their vivid properties such as low Curie temperature, high permittivity etc. Ferroelectric material $BaTiO_3$ is the most widely investigated material. Due to a high permittivity $BaTiO_3$, enables enhancement of the volumetric efficiency of multi-layer ceramic capacitors (MLCCs).

In this study $BaTiO_3$ has been synthesised by the co-precipitation method of chemical synthesis to get reduced particle/ crystallite size as compared to well existing synthesis methods such as solid state, sol-gel, hydrothermal methods. The XRD results reveal the proper formation $BaTiO_3$ along with crystalline size of 19.45 nm calculated from Scherrer formula, while SEM micrograph shows the agglomerated spherical particle of average size of 100-150 nm. The dielectric losses are more at 30^oC as compared to 100^oC for same frequency set. Variation of dielectric loss is checked at different frequencies in a common set of temperature shows that dielectric loss is very high for 10 KHz frequency as compared to 500 Hz and 1 KHz. The dielectric constant is more at 100^oC than at 30^oC for same frequencies. The dielectric constant is more for 500Hz and 100 KHz as compared to 10 KHz for same temperature set values. The resistance is higher at 30^oC as compared to 100^oC. The impedance remains almost same for both temperatures. The resistance and impedance decrease with increase in frequency.

Keywords: Ferroelectric, $BaTiO_3$, Co-precipitation Method, XRD, SEM, Dielectric Constant, Dielectric Loss, Resistance, Impedance.

CHAPTER 1

Introduction

1.1Ferroelectricity

When an electric field is applied to an ideal dielectric material there is no long-range transport of charge but only a limited rearrangement of charge such that the dielectric acquires a dipole moment and is said to be polarized. Atomic polarization, which occurs in all materials, is a slender displacement of the electrons in an atom relative to the nucleus. In addition, there is ionic polarization in ionic materials involving the relative displacement of cation and anion sub lattices. Dipolar materials, e.g. water etc. can become polarized because the applied electric field orients the molecules. Finally, space charge polarization involves a limited transport of charge carriers until they are stopped at a potential barrier and most probably a grain boundary or phase boundary.

An individual atom or ion in a dielectric is not subjected directly to an applied field but to a local field which has a very different value and under certain conditions. Further in feedback mechanism, lattice polarization produces a local field which lead to stabilizing the polarization further. The possibility of “spontaneous polarization” i.e., lattice polarization in the absence of an applied field arises due the fact. Such spontaneously polarized materials do exist and “ferroelectrics” constitute an important class among them [1]. The two conditions necessary in a material to classify it as a ferroelectric are (1) the existence of spontaneous polarization and (2) a demonstrated reorientation of the polarization by an applied electric field. Spontaneous polarization is defined as a stable polarization of a crystal in the absence of an external electric field.

The spontaneous polarization changes with temperature. There is a critical point—known as the Curie temperature—that defines the transition to a spontaneous polarization state from a state that is originally electrically neutral. The crystal is electrically neutral and its crystallographic phase is called paraelectric above the Curie temperature; below the Curie temperature, the crystal is spontaneously polarized and this crystallographic phase is called ferroelectric.

Amongst the 32 point groups or classes of crystals, 21 classes are non-centre symmetric and 20 of these are piezoelectric. One class, although lacking a center of symmetry is not piezoelectric due to other combined symmetry elements. Figure 1.1 shows that there are 10 crystal classes out of a possible 20 which are designated as pyroelectric material. Within a given temperature range, this group of materials possesses the unusual characteristic of being permanently polarized. Unlike the more general piezoelectric classes that produce a polarization under stress, the pyroelectrics develop this polarization spontaneously and form permanent dipoles in the structure. This polarization also changes with temperature and given the term pyroelectricity. A subgroup of the spontaneously polarized pyroelectric material is a very special category of materials known as ferroelectrics. Like pyroelectrics, materials in this group possess spontaneous polarization; however, unlike pyroelectrics, the direction of the spontaneous polarization is orientable by an electric field of some magnitude less than the dielectric breakdown of the material itself.

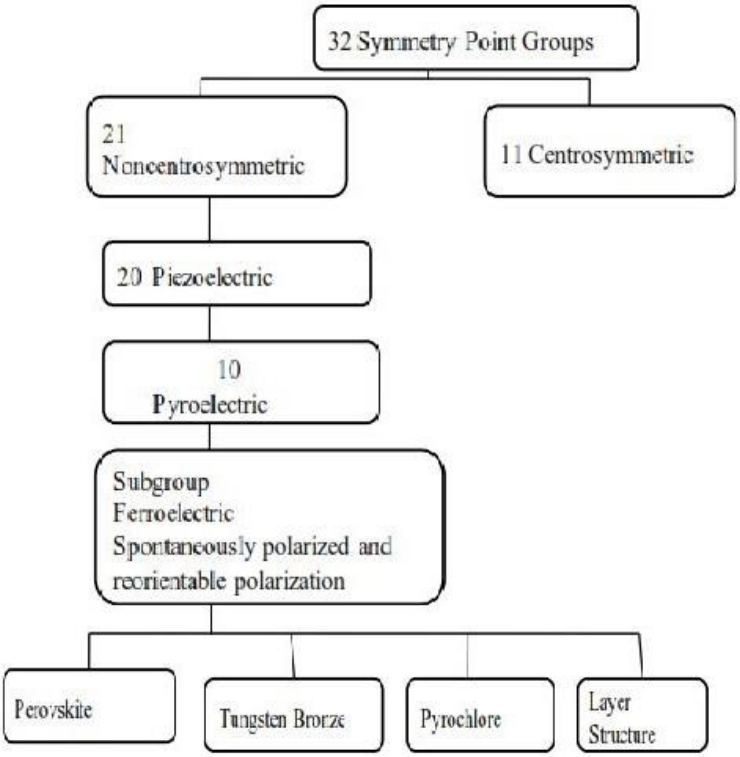

Fig.1.1 Interrelationship of piezoelectric and subgroups on the basis of symmetry.

Under the Curie temperature (T_c), ferroelectric crystals generally develop a random domain structure, leading to a net zero polarization of each crystal. Within each ferroelectric domain the polarization is in the same direction with a domain wall separating regions with different polarization directions. This structure is necessary to minimize free energy due to the development of anisotropic strains and depolarization fields below T_C. Domain walls are characterized by the angle between the polarization directions on either side of the wall. Thus a 180° domain wall demarks a boundary between antiparallel domains, while a 90° wall would be formed at the boundary between domains pointed "up" and "left", for example. The allowed angles for domain walls depend on the orientation of the spontaneous polarization allowed by symmetry. Thus in rhombohedrally distorted perovskites, there are no 90° domain walls like a tetragonal perovskite, but instead 71° and 109° walls. A more complete

picture of the way the polarization changes as a domain wall is crossed is given by Cao and Cross [2].

1.2 $BaTiO_3$

$BaTiO_3$ is the earliest piezoelectric transducer ceramic developed. Being isostructural with the mineral perovskite ($CaTiO_3$), $BaTiO_3$ is referred to as 'a perovskite'. Above its Curie point (approximately 130^oC) the unit cell is of cubic structure. Below the Curie point the structure is slightly distorted to the tetragonal form having a dipole moment along c direction. Other transformations occur at temperatures around 0^oC and -80^oC: for temperature lower than 0^oC the unit cell is orthorhombic with the polar axis parallel to a face diagonal and below -80^oC, the structure is rhombohedral with the polar axis along a body diagonal.

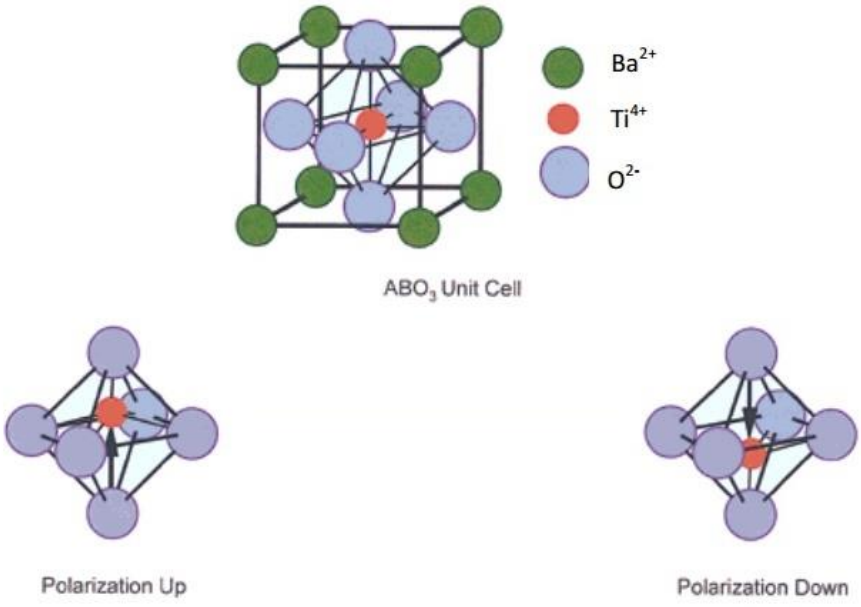

Fig.1.2 $BaTiO_3$ structure and polarizations

A typical ABO_3 with example of $BaTiO_3$ unit-cell structure is given in Fig.1.2. $BaTiO_3$ unit cell consists of a corner-linked network of oxygen octahedral with Ti^{4+}ions occupying sites within the octahedral cage and the Ba^{2+}ions situated in the interstices created by the linked octahedral. On application of electric field to this unit cell, the Ti^{4+}ion move to a new position as shown in the Fig.1.2. The figure also suggests 180° polarization reversal for two of the six possible polarization states produced by displacement of the central cation in the tetragonal plane of $BaTiO_3$.

Because the crystallite and, hence, the unit cell is randomly oriented and the ions are constrained to move only along certain crystallographic directions of the unit cell, generally, it is the case that an individual ionic movement only closely approximates an alignment with the electric field. However, when this ionic movement occurs, it leads to a macroscopic change in the dimensions of the unit cell and the ceramic as a whole. The change could be as big as a few tenths of a percent elongation in the direction of the field and approximately one-half of that amounts in the other two orthogonal directions. The orientation which is original but random of the domain polarization vectors (virgin condition) can be restored by heating the material above its T_c. This process is known as thermal depoling.

Also, as shown in Fig.1.2 the reversibility of the polarization is caused by the displacement of the central Ti^{4+}ion. The displacement is illustrated here as occurring along the c axis in a tetragonal structure, although it should be understood that it can also occur along the orthogonal a or b axes as well. The views of "polarization up" and "polarization down" (representing 180° polarization reversal) show two of the six possible permanent polarization positions.

Though $BaTiO_3$ is the first piezoelectric transducer ceramic ever developed, its use in recent years has shifted away from transducers to an almost exclusive use as high-

dielectric constant capacitors of the discrete and multilayer types. The reasons for this are primarily twofold: (1) its relatively low T_{cof} 130°C, which limits its use as high-power transducers, and (2) its low electromechanical coupling factor incomparison to PZT (0.52 vs 0.48), which limits its operational output.

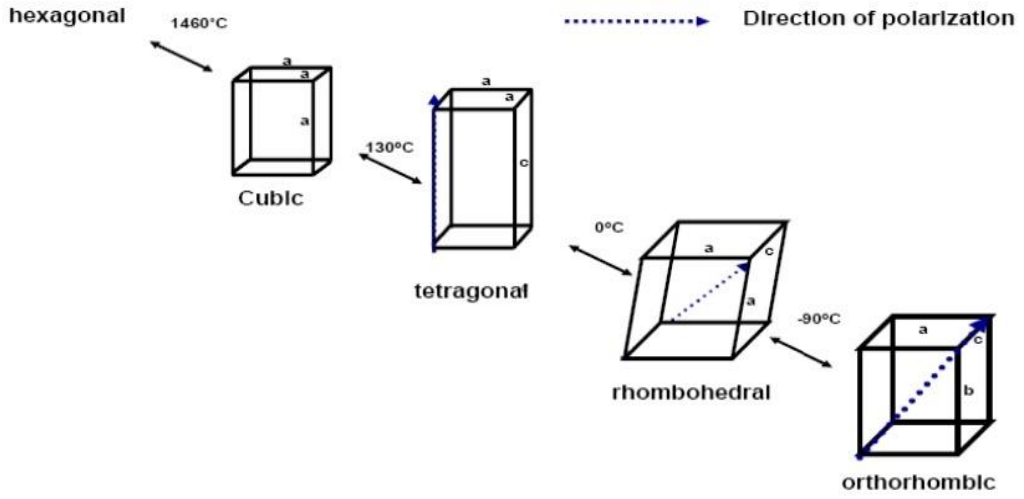

Fig.1.3 Phase diagram of $BaTiO_3$

$BaTiO_3$ assumes five different crystal structures namely, hexagonal, cubic, tetragonal, orthorhombic, and rhombohedral. The hexagonal and cubic structures are paraelectric while the tetragonal, orthorhombic and the rhombohedra forms are ferroelectric in nature.

Fig.1.3 shows hexagonal $BaTiO_3$ structure is stable above 1460^{o}C. Reconstructive hexagonal phase to cubic phase transformation occurs on cooling $BaTiO_3$ below 1460^{o}C. Of utmost important parameter relating to its dielectric application is the ferroelectric - paraelectric transition which occurs at the Curie temperature (around 130^{o}C). At this temperature, paraelectric cubic $BaTiO_3$ transforms into the ferroelectric tetragonal structure following an elongation along an edge. The tetragonal phase is

stable until 0^{o}C, where it transforms into the orthorhombic phase by elongation along a phase diagonal. Finally, there is a low temperature transition at - 90^{o}C where the orthorhombic phase transformed to the rhombohedral phase. It is used for this application due to its high dielectric constant and low dielectric loss.

1.3 Applications

1. In the field of specific electronic ceramics such as MLCC and microwave dielectric ceramic
2. As nanoscale modules for the assembly of electronic devices, such as detectors, capacitors, and sensors
3. In multifunctional structural capacitors where the material elements have to simultaneously carry load and store energy
4. In high-density optical data storage
5. In phase conjugated mirrors and lasers
6. In nonlinear optical devices
7. In pattern recognition, and micro-capacitors
8. In optical computing, optical image processing, piezoelectric devices, pyroelectric sensors, semiconductive ceramics, varistors, electro-optic devices.
9. In dielectric amplifiers and dynamic holography.

CHAPTER 2

Literature Review

2.1 Synthesis Methods OF Barium Titanate

Barium Titanate ($BaTiO_3$) was synthesized through different techniques by various researchers. The selected techniques for synthesizing barium titanate depend on cost as well as applications. The quality of the powders is not only influenced by the synthesis route but also by the starting materials taken for the process. As miniaturization of electronic devices continues to demand smaller particle size powders with controlled morphology, the desired characteristics of the starting powder is a very critical issue [3]. The successful synthesis of barium titanate powder with their unique dielectric properties largely depends on the purity and crystal structure that greatly influences final properties [4,5].

In general there are two types of methods for the synthesis of $BaTiO_3$

1. Solid state method.
2. Sol-Gel method
3. Hydrothermal Method
4. Mechanochemical synthesis
5. Combustion synthesis
6. Molten salt Method

2.1.1 Conventional solid-state reaction

Barium Titanate can be prepared by a solid-state reaction that involves ball milling of $BaCO_3$ or BaO and TiO_2 which requires calcination of the mixture at high temperature. Some researchers reported that the needed calcination temperature was as

high as 800 ^{o}C to 1200^{o}C [6,7,8]. Barium titanate powders prepared by a solid-state reaction are highly agglomerated, with a large particle size (2-5 μm) and high impurity contents due to their inherent problems such as high reaction temperature, heterogeneous solid phase reaction, resulting in poor electrical properties of the sintered ceramics [9].

Manzoor et al [10] reported that the Size control of $BaTiO_3$ was prepared in the reaction between $BaCO_3$ and TiO_2. Smaller TiO_2 particles have higher surface area leading to faster initial reaction. $BaCO_3$ particles which are mechanically milled accelerate the diffusion process and decreased the calcinations temperature. They reported that nano-sized $BaTiO_3$ particles with about 60 nm can synthesized by using the conventional solid-state reaction between $BaCO_3$ and TiO_2.

2.1.2 Sol-Gel method

Sol-gel is a method for preparing metal oxide glasses and ceramics by hydrolyzing a chemical precursor to form a sol and then a gel, which on drying (evaporation) and pyrolysis gives an amorphous oxide.

Wang et al [11] used two typical wet-chemistry synthesis methods such as stearic acid gel and acetic acid gel. Both the methods were prepared $BaTiO_3$powder calcined at 550^{o}C by SAG and 800^{o}C by AAG respectively which has a cubic perovskite structure. They observed different grain size distributions within 25–50 nm for SAG and 50–80 nm for AAG. The particles were almost irregular in shape and agglomerate seriously due to high synthesis temperature in case of AAG. SAG has no Ba and Ti losses, and no halide anions and alkali-metal cations introduced or generated in the course of reaction, thus, SAG is one of most effective and convenient way to synthesize $BaTiO_3$ nanopowders.

Xueguanget.al [12] used sol-precipitation process which does not require further thermal treatment of the product, such as calcination or annealing due to enhance the homogeneity of crystals and their growth. However, single-crystal $BaTiO_3$ nanoparticles can be directly obtained at the low temperature of 80^oC and a strong alkaline condition rather than amorphous gel that often formed in the standard sol-gel process. They found nanoparticles with an average diameter of about 20 nm using Transmission electron microscopy.

Cheung et al.[13] prepared $BaTiO_3$ powders and films by a sol-gel method. This method involved the mixing of titanium isopropoxide and barium acetate in deionized water under continuous stirring at room temperature. They found crystallite size is around 20-35nm and the room temperature relative permittivity of the films (measured at 1 kHz) annealed at 700, 750,800 and 850°C were 207, 225, 367 and 401 respectively. They also observed that the values of the remanent polarization, spontaneous polarization and coercive field of the film annealed at 850°C were $5mC/cm^2$, $10mC/cm^2$ and 70kV/cm, respectively.

Hwang et.al [14] synthesized spherical $BaTiO_3$ particles by the sol- gel method at 45°C. The (Ba–Ti) gel used as a starting material was prepared by aging mixtures of titanyl acylate with a barium acetate aqueous solution. Potassium hydroxide (KOH) was used as a catalyst for the formation of $BaTiO_3$. They found fully crystallized spherical $BaTiO_3$ powder with a particle size of 40–250 nm which is formed at the very low reaction temperature of 45°C.They also observed that the final particles formed via aggregation of the fine particles that seem to be the primary particles of bulk (Ba–Ti) gel.

2.1.3 Hydrothermal Method

The hydrothermal method is also used for synthesizing $BaTiO_3$ powder. Ciftci et al [15] synthesized $BaTiO_3$ powder by the hydrothermal method at temperatures between ~100-200^oC by reacting fine TiO_2 particles with a strongly alkaline solution (pH>12) of Ba $(OH)_2$. $TiCl_4$, titanium alkoxide and TiO_2 gels were used as titanium sources at reaction temperatures in the range of 100-400^oC. They found particle size of $BaTiO_3$ in the range of 50-400 nm.

Boulos et al [6] synthesized $BaTiO_3$ powders by the hydrothermal method using two different titanium sources $TiCl_3$ and TiO_2. The barium source was $BaCl_2 \cdot 2H_2O$. They synthesized $BaTiO_3$ at two temperatures, namely 150^oC and 250^oC. They observed that SEM micrographs of barium titanate powders show spherical highly crystallized elementary grains with sizes in the range 40-70 nm for samples prepared from $TiCl_3$ at 150^oC and 80-120 nm at 250^oC. The average particle size for powders obtained from TiO_2 at 150^oC or 250^oC was 40-70 nm.

Liu et al. [17] prepared $BaTiO_3$ by the microwave method and evaluated its sinterability, structure and dielectric properties in comparison to samples prepared by conventional hydrothermal processing. Starting reagents were Ba $(NO_3)_2$, $TiCl_4$ and KOH. All chemical reactions were conducted in a microwave digestion system. The system is controlled by pressure and the parameters which were varied include pressure (and thus, temperature) and time. They found that SEM analysis of powders prepared by both hydrothermal methods yielded a particle size of about 0.2 μm. Thus cubic $BaTiO_3$ powders can be prepared by the microwave method for about half an hour, but in the case of conventional hydrothermal route for two and half hours.

Guo et al. [18] observed that the microwave hydrothermal method can obtain the desired $BaTiO_3$ powder in a shorter time and at a lower temperature (30 min, 80^oC) than the conventional hydrothermal method (5h, 150^oC).

Sasirekha et al. [19] synthesized nanosized barium titanate powders by a hydrothermal method. They studied the effect of titania precursors on the phase transition of $BaTiO_3$ with respect to Ba/Ti ratio, reaction parameters i.e. temperature and time, and calcination temperature. They observed $BaTiO_3$ in pure cubic phase with spherical morphology with a lower calcination temperature, Ba/Ti ratio, reaction temperature, and time.

2.1.4 Mechanochemical synthesis

Stojanovic et al [20] prepared $BaTiO_3$ by mechanochemical synthesis, starting from barium oxide (BaO) obtained from thermally treated $BaCO_3$. According to the following reaction

$BaCO_3 \rightarrow BaO + CO_2$

in air at 900^oC/4h, and titanium oxide (TiO_2) in a crystal form.

Mechanochemical activation, i.e. mechanochemical synthesis was performed in a planetary ball mill in an air atmosphere for up to 4h, using a zirconium oxide vial and zirconium oxide balls as the milling medium. They identified strong agglomeration of powders after milling for 4h. $BaTiO_3$ powder consisted of particle agglomerates of varying size and morphology, with grains of a mostly rounded shape in the range of 20-50 nm.

Xue et al. [21] synthesized a perovskite $BaTiO_3$ phase in an oxide matrix that consists of BaO and TiO_2 by mechanical activation, without any additional heat treatment in a nitrogen atmosphere. They found that $BaTiO_3$ powder exhibits a well-established

nanocrystalline structure with crystallite size of ~ 14 nm and an average particle size of 20–30 nm for the activation derived $BaTiO_3$ powder.

2.1.5 Combustion synthesis

Luo et al [22] prepared nanosized tetragonal barium titanate by low-temperature combustion synthesis process (LCS). They produced tetragonal $BaTiO_3$ with high purity at low ignition temperature (~300°C) and the crystalline size of the powder obtained was found to be less than 50 nm.

Won et al [23] synthesized tetragonal and submicron barium titanate particles from the BaO_2–TiO_2–C mixture through a low temperature isothermal heat treatment utilizing combustion synthesis technique. They found that precursor powder prepared by the combustion method easily transformed to the tetragonal $BaTiO_3$ starting from 700°C. They also found that the formation of tetragonal $BaTiO_3$ powder at low temperature is conditioned by high chemical activity and specific characteristics of combustion products. $BaTiO_3$ specimens were found to possess high dielectric constant and low dissipation factor at room temperature.

Anuradha et al [24] studied the combustion synthesis of nanostructured barium titanate. Various samples of $BaTiO_3$ were prepared by the solution combustion of three different barium precursors (BaO_2, $Ba(NO_3)_2$ and $Ba(CH_3COO)_2$) and fuels such as carbohydrazide (CH), glycine (GLY) or citric acid (CA) in the presence of titanyl nitrate. They observed particle size of $BaTiO_3$ in the range of 10–50 nm , crystal structure in Cubic $BaTiO_3$ and crystallite size in the range of 50-60nm.

2.1.6 Molten salt Method

The reaction mechanism of a given phase in the MSS is little different from that of the solid-state reaction, as long as the salt intervenes in the formation reaction of the required phase. [16]

Oxides corresponding to a perovskite compound are mixed with one or two kinds of salt and then fired at a temperature above the melting point of the salt to form a flux of the salt composition.

At this temperature, the oxides are rearranged and then diffused rapidly in a liquid state of the salt. On further heating, particles of the perovskite phase are formed through the nucleation and growth processes.

Gorokhovsky et al [25] studied the prepared $BaTiO_3$ by treatment of TiO_2 powder in molten mixtures of KNO_3–Ba $(NO_3)_2$–KOH. The products were characterized by different ratios of $BaTiO_3/TiO_2$. The rate of $BaTiO_3$ formation was not influenced by the temperature of treatment in the range of 450–550^oC. Lower temperatures and longer times of treatment are preferable because of the higher stability of nitrate ions in the melt. If the chemical composition of the product must be controlled, the large particles of barium polytitanates could be eliminated from the suspension by using fine filter paper.

Rorvik et al [26] prepared $BaTiO_3$ nanorods by molten salt synthesis route to elucidate the role of volatile chlorides. A precursor mixture containing barium (or lead) and titanium was annealed in the presence of NaCl at 760 or 820°C. The main products were respectively isometric nanocrystalline $BaTiO_3$. They found that NaCl reacted with BaO resulting in loss of volatile $BaCl_2$ and formation and preferential growth of titanium oxide-rich nanorods instead of the target phase $BaTiO_3$.

Jeffrey et al [27] synthesized $BaTiO_3$ by solution-phase decomposition of bimetallic alkoxide precursors in the presence of coordinating ligands. They observed that the reaction yieldswell-isolated nanorods with diameters ranging from 5 to 60 nm and lengths reaching up to >10 μm. These nanorods are composed of single-crystalline cubic perovskite $BaTiO_3$.

Liu et al [28] synthesized single crystalline $BaTiO_3$ nanoparticles starting from $BaCO_3$ and TiO_2 by a composite-hydroxide-mediated method. They found all $BaTiO_3$ samples of cubic phase with size from 70 to100 nm under different reaction temperature (165–220 °C) and time (24–72 h); higher temperature and longer time clearly favored the increase of particle size.

Yuanbing et al [29] prepared single-crystalline $BaTiO_3$ nanowires with a novel and simple one-step solid-state chemical reaction in the presence of NaCl at 820^{o}C and a nonionic surfactant. They scaled up this process to produce grams of single crystalline $BaTiO_3$ nanomaterials. They found nanowires of about 50-80 nm in diameter, and their lengths range from 1.5 μm to even longer than 10 μm. They also observed the purity and crystallinity of the as-prepared samples using powder XRD.

2.2 Sintering Behavior

Wang et al [30] investigated the preparation of bulk dense nanocrystalline $BaTiO_3$ ceramics using an unconventional two-step sintering strategy, which offers the advantage of not allowing grain growth while increasing density from about 73 to above 99.6%.The kinetics of unconventional two-step sintering method exploits the different kinetics between densification diffusion and grain boundary mobility. By using this method, bulk dense ceramics with a grain size of 8–10 nm was obtained successfully at a very low sintering temperature.

Yinget al [31] prepared nanometer-scale barium titanate ($BaTiO_3$) powders via a process consisting of chemical dispersion and physical grinding/mixing. The nano-$BaTiO_3$ was sintered at the temperatures ranging from 1100 to 1300°C for various time spans. The $BaTiO_3$ sample sintered at 1100°C for 6 h possesses relatively small grain sizes (about 140 nm), high density (about 95% T.D.) and distinct room-temperature dielectric properties (dielectric constant = 8000;dielectric loss = 5×10^{-3}).

Polotai et al [32] developed a novel approach to pressureless sintering based on the combination of rapid-rate, rate controlled and two-step sintering under a controlled atmosphere conditons. This combined sintering method facilitates control of grain/pore morphology. The application of this sintering approach for pure nanocrystalline barium titanate powder enables the suppression of grain growth during the intermediate and final stages of sintering and the production of fully dense ceramics with 108 nm grain size. The grain growth factor was 3.5, which was 3 and 17 times lesser than rate-controlled and conventional sintering, respectively.

2.3 Dielectric Behavior

Shi et al [33] studied the dielectric properties of barium titanium ceramics fabricated with fine powders (about 40 nm) with that fabricated with micro-size coarse powders (about 2 mm). They fabricated three kinds of ceramics; one using pure nano-size fine powders, pure micro-size coarse powders, and using the combination of both. The sintering temperature of the ceramics with pure nano-size fine powders is 150°C lower than that with pure micro-size coarse powders. The relative density of the ceramics increases with the amount of nano-size fine powders for the same sintering conditions. The grain size of the ceramics body with pure micro-size coarse powder is about 5 mm, but that of pure nano-size fine powder is about 1 mm. The room temperature

dielectric constant of the ceramics increases with the increasing of the amount of nanosized fine powder. For pure nano-size fine powders, dielectric constant is about 5000 at room temperatures, and that of micro-size coarse powders is about 2200.

Park et al [34] used various particle sizes of starting barium titanate in order to examine effect of grain size and external stress on the dielectric temperature characteristics of barium titanate. The grain size was proportional to the particle size of starting barium titanate. The dielectric temperature characteristics of the small grains (< 4 μm) was less sensitive to the grain size in comparison with those of the large grains (> 4 μm), which was attributable to the internal stress. It was also suggested that stress is one of the origins of diffuse phase transition (DPT).

Arlt et al [35] studied the dielectric properties, structural and microstructural proeprties of ceramic $BaTiO_3$ indicating the sizes of grains of the order of 0.3-100 μm . At grain sizes <10 μm, the width of ferroelectric 90°domains decreases proportionally to the square root of the grain diameter. The smaller the grains, the more the dielectric and the elastic constants are determined by the contribution of 90° domain walls. The permittivity below the Curie point showed a pronounced maximum ε_r ~5000 at grain sizes 0.8-1 μm. At grain sizes <0.7 μm the permittivity strongly decreases and the lattice gradually changes from tetragonal to pseudocubic.

Begget al [36] studied the room-temperature tetragonal-to-cubic transformation in $BaTiO_3$ powders with decreasing particle size, using materials prepared mainly by hydrothermal methods. It is observed that hydrothermal $BaTiO_3$ powders exhibit a uniform particle size distribution. The tetragonal-to-cubic transformation temperature was found to lie in the range of 121°±3 °C for $BaTiO_3$ powders with room temperature values >1.008.

Liet al [37] showed that clustering is an important effect on the tetragonal-cubic transformation of barium titanate ($BaTiO_3$) particles. Small particles that would be cubic, are tetragonal if they are in a cluster. The effects of clustering had been studied on the c/a ratio of the particles and the enthalpy change (ΔH) of transition as a function of particle size. At a smaller particle, the c/a ratio and the value of ΔH both decrease size than those which are observed in samples where clustering is minimal. The results were consistent with the observation that very small grains in polycrystalline samples can remain tetragonal even though the grain size is so small that it would be cubic if it were an individual particle. The transition temperature, T_C, on the other hand, is insensitive to the particle size, which is similar to the observation in polycrystalline $BaTiO_3$ that T_c is insensitive to the grain size. The observed clustering effect is suggested to result from the reduction of depolarization energy of particles in clusters.

CHAPTER 3

Synthesis and Characterization of $BaTiO_3$

3.1 Materials used for the synthesis of $BaTiO_3$

The compounds barium acetate [$Ba(CH_3COO)_2.xH_2O$], titanium tetrachloride [$TiCl_4$] and ethanol [C_2H_5OH] are used for the synthesis of $BaTiO_3$ in the process.

3.2 Procedure

The process used for the synthesis is chemical co-precipitation method. Barium Acetate is mixed with ethanol. It is magnetically stirred at temperature of 60-80^oC which results in white paste. The paste formed is cooled to room temperature. On the other hand, $TiCl_4$ is diluted with ethanol and magnetically stirred at room temperature. The solution thus formed is mixed with the white paste formed earlier from barium acetate and ethanol solution. The solution is again magnetically stirred for 1-2 hr while gradually increasing the temperature. A white powder is formed, and is collected.

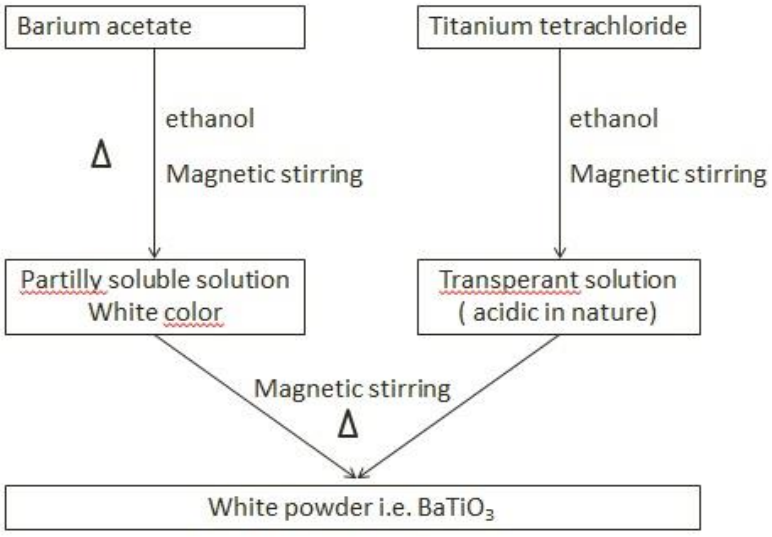

Fig.3.1 Flow chart of synthesis method

The powder i.e. $BaTiO_3$ is then heated in various stages to remove the by-products of the reaction.

Firstly, it is heated at 100^oC to remove any residual ethanol. As the boiling point of ethanol is 78.37^oC, it evaporates from the powder. The calcination is done at 600^oC for 4 hours to obtain $BaTiO_3$ after eliminating the by-products.

A pellet can be made out of the material and sintered at 800^oC for 2 hours for various characterizations.

3.3 Structural Analysis

3.3.1 DSC (Differential Scanning Calorimetry)

Differential scanning calorimetry (DSC) is a thermo-analytical technique in which the difference in the amount of heat required to increase the temperature of a sample and reference is measured as a function of temperature. Both the sample and reference are maintained at nearly the same temperature throughout the experiment. In general, the temperature program for a DSC analysis is designed such that the sample holder temperature increases linearly as a function of time. The reference sample should have a well-defined heat capacity over the range of temperatures for which it is to be scanned. The DSC of the sample was done upto 550^oC.

3.3.2 XRD (X-Ray Diffration)

The diffraction of X-rays by matter results from the combination of two different phenomena: (a) scattering by each individual atom, and (b) interference between the waves scattered by these atoms. This interference occurs because the waves scattered

by the individual atoms are coherent with the incident wave, and therefore between themselves as shown in Fig 3.2.

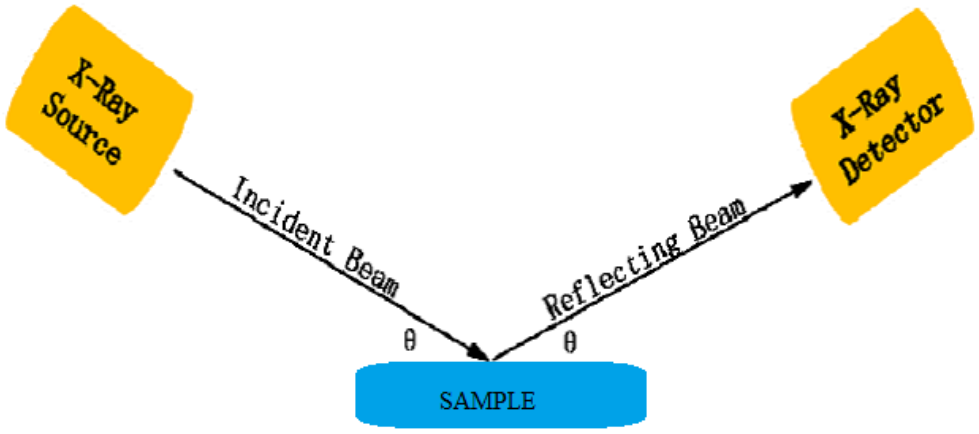

Fig. 3.2 Diagram of incident angle and reflecting angle with respect to the normal of the diffracting for X-Ray Diffraction.

In 1912, W. L. Bragg recognized a predictable relationship among several factors.

1. The distance between similar atomic planes in a mineral (the interatomic spacing) which we call the *d*-spacing and measure in angstroms.
2. The angle of diffraction which we call the theta angle and measure in degree. For practical reasons the diffractometer measures an angle twice that of the theta angle.
3. The wavelength of the incident X-radiation of Cu-K_{α}, symbolized by the Greek letter lambda and, in this thesis, equal to 1.54 angstroms.

These factors are combined in Bragg's Law:

$$n\lambda = 2d \sin\theta \quad \text{(Eq. 3.1)}$$

Where n is an integer, λ is the wavelength of X-rays, d is the lattice interatomic spacing and θ is the diffraction angle.

The XRD was used in this thesis to identify the changes of the crystal structure in my samples after sintered at different temperature. The scanning of the 2θ angle was started at 20°, and ended at 80°. The scanning rate was 0.2°/min.

3.3.3 SEM (Scanning Electron Microscope)

A focused beam of high-energy electrons to generate a variety of signals at the surface of solid specimens is used in the scanning electron microscope (SEM). The signals deriving from electron-sample interactions reveal information about external morphology (texture), chemical composition, and crystalline structure and orientation of materials making up the sample. In most applications, data is collected over a selected area of the surface of the sample, and a 2-dimensional image is generated displaying spatial variations in the properties. The SEM is also capable of performing analyses of selected point locations on the sample. The grain size of the sample is calculated using SEM image.

3.4 Electric Measurement

3.4.1 Conductivity and Dielectric Measurements

An LCR meter is used for conductivity and dielectric measurements. An LCR meter is a piece of electronic test equipment used to measure the inductance (L), capacitance (C), resistance (R), impedance (Z) of a component.

In the simpler versions of this instrument the true values of these quantities are not measured; rather the impedance is measured internally and converted for display to the corresponding capacitance or inductance value. Readings will be reasonably accurate if the capacitor or inductor device under test does not have a significant resistive component of impedance. More advanced designs measure true inductance or capacitance, and also the equivalent series resistance of capacitors and the Q factor of inductive components.

Usually the device under test (DUT) is subjected to an AC voltage source. The meter measures the voltage across and the current through the DUT. From the ratio of these the meter can determine the magnitude of the impedance. The phase angle between the voltage and current is also measured in more advanced instruments; in combination with the impedance, the equivalent capacitance or inductance, and resistance, of the DUT can be calculated and displayed. The meter must assume either a parallel or a series model for these two elements. The most useful assumption, and the one usually adopted, is that LR measurements have the elements in series (as would be encountered in an inductor coil) and that CR measurements have the elements in parallel (as would be encountered in measuring a capacitor with a leaky dielectric). An LCR meter can also be used to judge the inductance variation with respect to the rotor position in permanent magnet machines (however care must be taken as some LCR meters can be damaged by the generated emf produced by turning the rotor of a permanent-magnet motor).

Inductance, capacitance, resistance, and dissipation factor can also be measured by various bridge circuits. They involve adjusting variable calibrated elements until the signal at a detector becomes null, rather than measuring impedance and phase angle.

In their early days, commercial LCR bridges used a variety of techniques involving the matching or "nulling" of two signals obtained from a single source. The first signal was generated by applying the test signal to the unknown material and the second signal was generated by using a combination of known/standard R and C values. The signals were summed through a detector (normally a panel meter with or without some level of amplification). When zero current was noted by changing the value of the standards and looking for a "null" in the panel meter, it could be assumed that the current magnitude through the unknown was equal to that of the standard and that the phase was exactly the reverse (180 degrees apart). The combination of standards selected could be arranged to read out C and D directly which was the precise value of the unknown standard.

Bench top LCR meters typically have selectable test frequencies of more than 100 KHz. They often include possibilities to superimpose a biasing DC voltage or current on the AC measuring signal. Lower end meters offer the possibility to externally supply these DC voltages or currents while higher end devices can supply Dc voltage or current internally. In addition bench top meters allow the usage of special fixtures to measure SMD components, air-core coils or transformers.

Aligent 4284A LCR meter is used to measure capacitance, dielectric losses, resistance and impedance of the sample at various temperatures ranging from room temperature i.e. 30^{o}C to 300^{o}C and frequency ranging from 20Hz to 1MHz.

CHAPTER 4

Results and Discussion

4.1 Differential Scanning Calorimetry (DSC)

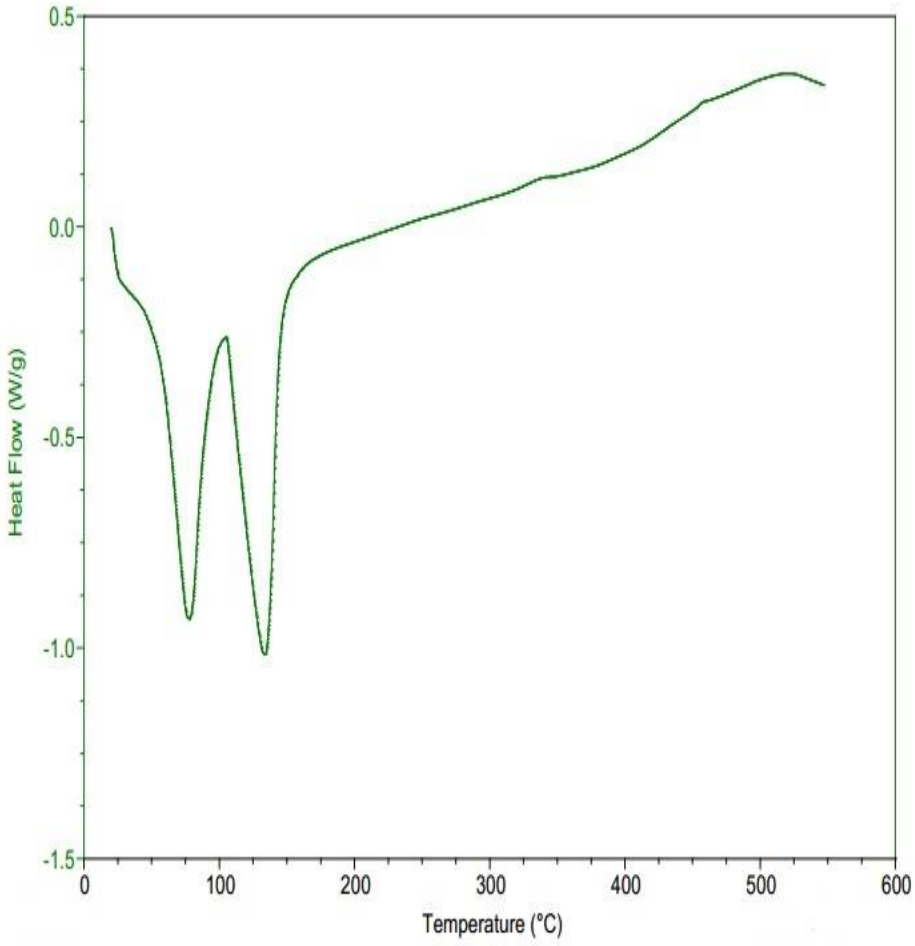

Fig.4.1 The DSC of raw sample of $BaTiO_3$

The DSC of raw sample of $BaTiO_3$ has been observed as shown in Fig.4.1 from room temperature to 540^{o}C. There is a change in heat flow at around different temperatures i.e. 80^{o}C, 100^{o}C, 140^{o}C, 350^{o}C, 460^{o}C, 540^{o}C.

The change in heat flow shows some change in material or its composition. The heat flow changes at various temperatures signify different changes as listed below in Table 4.1.

Table 4.1 Changes at different temperatures as observed in DSC.

Temperature (in ^{o}C)	Change
80	Evaporation of ethanol
100	Boiling of water content
130-140	Curie temperature of $BaTiO_3$ resulting in structural change
350	Starting of phase formation of $BaTiO_3$
460	Partial phase formation of $BaTiO_3$
540	Phase formation of $BaTiO_3$

4.2 XRD(X Ray Diffraction)

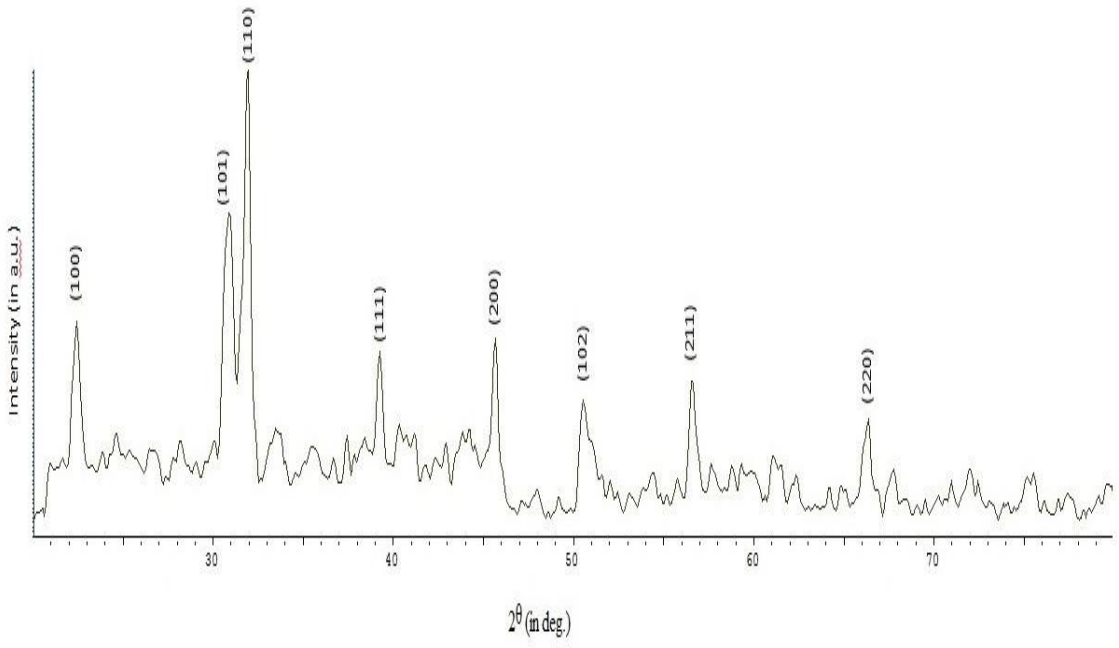

Fig.4.2 X Ray Diffraction (XRD) pattern of $BaTiO_3$ calcined at 600^{o}C for 4 hours

The XRD pattern of calcined $BaTiO_3$ at 600^oC for 4 hours is shown in Fig 4.2. The existing peaks are matched with the JCPDS reference code 00-005-0626. It shows the formation of tetragonal structure with the space group of the prepared $BaTiO_3$ is P4mm and the space group number 99. The lattice parameters observed for the pattern are given in Table 4.2.

Table 4.2 Lattice parameters and their values.

Parameters	**Value**
a (Å):	3.9940
b (Å):	3.9940
c (Å):	4.0380
Alpha (°):	90.0000
Beta (°):	90.0000
Gamma (°):	90.0000

The crystallite size calculated from Scherrer's formula is observed as shown in Table 4.3. The average crystallite size is 19.45 nm.

Table 4.3 Crystallite size of $BaTiO_3$ calcined at 600^oC for 4 hrs at various 2θ values

2θ (in deg.)	**Crystallite Size (in nm)**
22.437	12.09
30.872	12.31
31.906	22.14
39.255	22.04
45.620	24.34
50.587	09.18
56.642	31.44
66.318	22.04

4.3 SEM(Scanning Electron Microscopy)

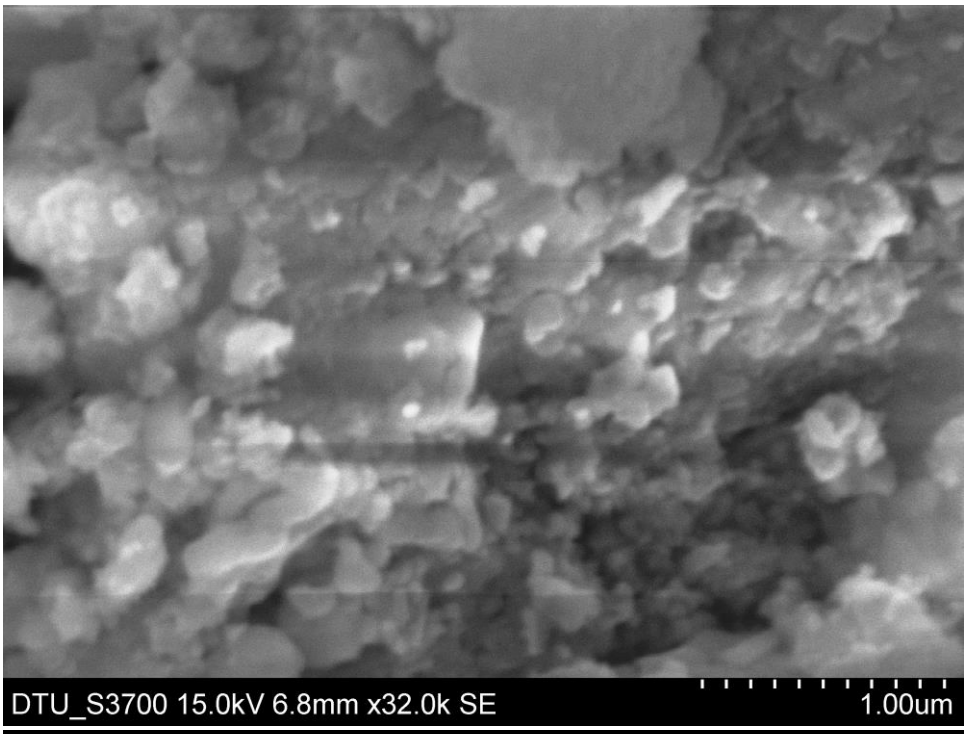

Fig 4.3 SEM image for $BaTiO_3$ calcined at 600^oC

The SEM image obtained for the prepared $BaTiO_3$ sample as shown in Fig.4.3. The SEM image indicats the agglomerated and bit spherical particle of size lies in between 100-150 nm.

4.4 Electrical Characterization

In electrical characterizations of the prepared material, dielectric losses, dielectric constant, resistance and impedance are measured for different sets of frequencies i.e. from 20Hz to 1MHz and temperatures i.e. 30^oC and 100^oC. The variation of dielectric constant with frequency is observed at these temperatures and shown in Fig.4.4 (a).

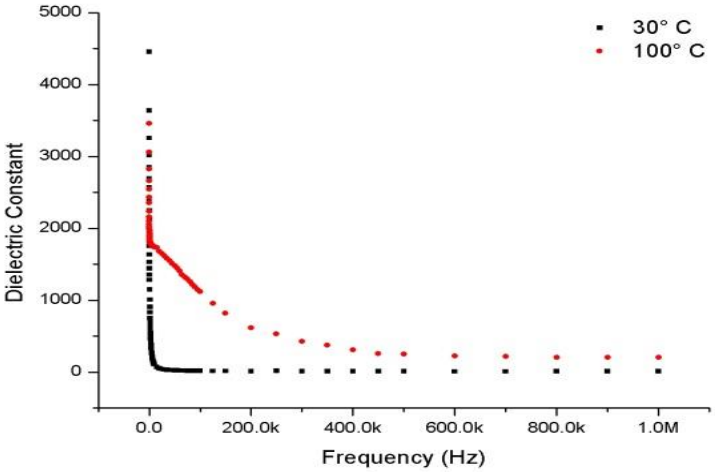

Fig.4.4 (a) Variation of dielectric constant with frequency at 30^{o}C and 100^{o}C for $BaTiO_3$ calcined at 600^{o}C.

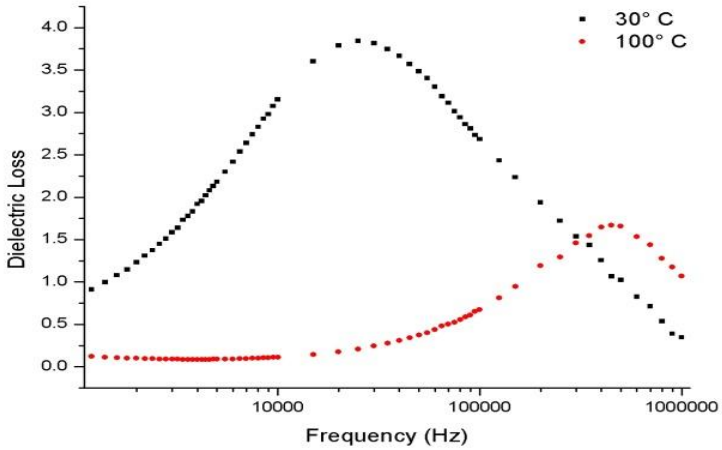

Fig.4.4 (b) Variation of dielectric constant with frequency at 30^{o}C and 100^{o}C for $BaTiO_3$ calcined at 600^{o}C.

From the observation, it is found that the dielectric constant for the same set of frequencies is more at 100^{o}C than 30^{o}C.

The variation of dielectric loss with frequency has also been observed for both the temperatures 30^{o}C and 100^{o}C as shown in fig.4.4 (b). It is found that the dielectric losses are more at 30^{o}C as compared to losses at 100^{o}C at same frequencies.

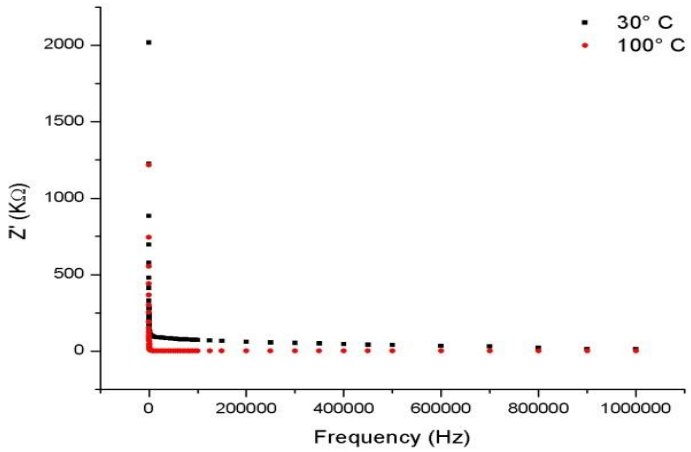

Fig.4.5 (a) Variation of resistance (Z') with frequency at 30°C and 100°C for $BaTiO_3$ calcined at 600°C.

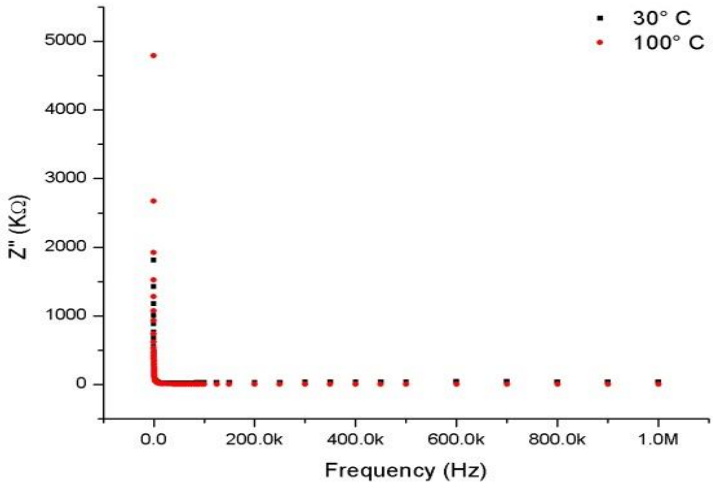

Fig.4.5 (b) Variation of impedance (Z'') with frequency at 30°C and 100°C for $BaTiO_3$ calcined at 600°C.

From Fig 4.5 (a), variation of resistance with frequency indicate that the resistance is higher at 30°C than 100°C, especially at lower frequencies. However, Fig 4.5 (b) shows the impedance is almost same for both temperatures 30°C and 100°C.

Another inference which can be drawn from Fig 4.5 (a) and (b) is that resistance and impedance decrease with increase in frequency.

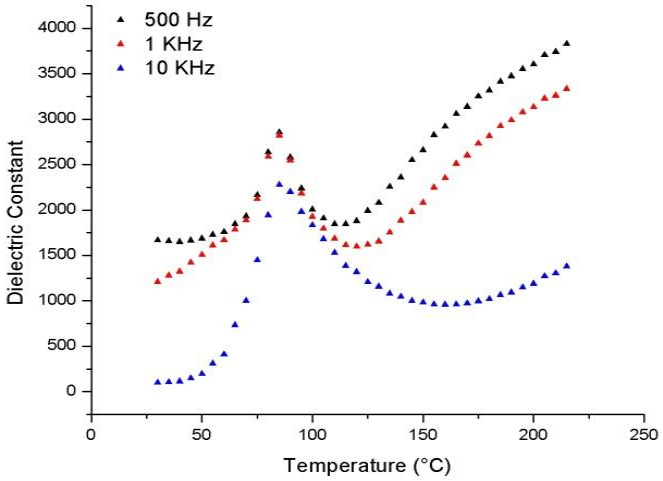

Fig.4.6 (a) Variation of dielectric constant with temperature at 500Hz, 1 KHz and 10 KHz for $BaTiO_3$ calcined at 600^oC.

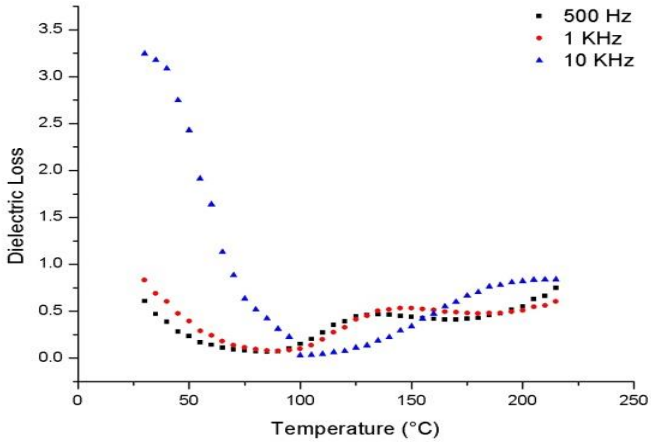

Fig.4.6 (b) Variation of dielectric loss with temperature at 500Hz, 1 KHz and 10 KHz for $BaTiO_3$ calcined at 600^oC.

Fig 4.6 (a) indicates the behavior of the dielectric constant with temperature for different frequencies as a characteristic ferroelectric material. It reveals that the dielectric constant is more for 500Hz and 1 KHz as compared to 10 KHz. The dielectric loss is quiet high for 10 KHz frequency as compared to 500 Hz and 1 KHz, as represented in Fig 4.6(b).

CHAPTER 5

Summary and Conclusion

Barium Titanium Oxide is prepared by co-precipitation method, one of the chemical methods, using barium acetate and titanium tetrachloride with ethanol (dil.) as solvent. The XRD pattern confirms the material to be $BaTiO_3$ with particle size or crystallite size of 19.45 nm. While SEM image shows that the particle size thus obtained is 100-150 nm. The electrical characterizations show that particle is ferroelectric. The dielectric losses are more at 30^oC as compared to 100^oC for same frequency set and when variation of dielectric loss is checked at different frequencies in a common set of temperature, it is observed that dielectric loss is very high for 10 KHz frequency as compared to 500 Hz and 1 KHz. On other hand, the dielectric constant is more at 100^oC than at 30^oC for same frequencies. The dielectric constant is more for 500Hz and 100 KHz as compared to 10 KHz for same temperature set values. The resistance is higher at 30^oC as compared to 100^oC, especially at lower frequencies. The impedance remains almost same for both temperatures. The resistance and impedance decrease with increase in frequency.

REFERENCES

1. Moulson A.J. and Herbert J.M., Electroceramics Materials properties applications, Chapman and Hall, London, 52, 1990, 18.
2. Cao W. and Cross L.E., Physical Review B, 44, 1991, 5.
3. Lee B.I., Wang M., Yoon D., Hu M., Journal of Ceramic Production Research, 4, 2003, 17.
4. Haertling G.H., Journal of American Ceramics Society, 82, 1999, 797.
5. Vinothini V., Singh P., Ceramics International, 32, 2006, 99.
6. Boulos M., Guillement-Fritsch S., Mathieu F., Durand B., Lebey T., Bley V. Solid State Ionics, 176 , 2005, 1301.
7. Potdar H.S., Deshpande S.B., Date S.K., Materials Chemistry, 58, 1999, 121.
8. Simon-eveyrat L., Hajjaji A., Emziane Y., Guiffard B., Guyomar D., Ceramics International ,33 , 2007, 301.
9. Wu Long, Ming-Cheng Chure, King-Kung Wu, Wen-Chung Chang, Ming-Ju Yang WeiKuo Liu , Menq-Jion Wu, Ceramics International, 35 , 2009, 957.
10. Manzoor U. and.Kim D.K., Journal of Material Science and Technology, 23, 2007, 47.
11. Wang L., Liu L., Xue D., H. Kang, C. Liu, Journal of Alloys and Compounds, 440 , 2007, 78.
12. Xueguang. He ,Fan Guangneng, , Huangpu Lixia ,Journal of Crystal Growth 279, 2005, 489.
13. Cheung M.C., Chan H.L.W., Zhou Q.F.,Choy C.L, Nano Structured Materials, 11, 1999, 837.

14. Un-Yeon Hwang, Hyung-Sang Park, and Kee-Kahb Koo, Journal of American Ceramics Society, 87, 2004, 2168.

15. Ciftci .E., Rahaman M. N., Journal Of Materials Science 36 , 2001, 4875 .

16. Yoon Kihun, Cho Yong Soo, Kang Dong Heon , Journal of Materials Science 33 , 1998, 2977.

17. Liu Shi-Fang, Isaac Abothu Robin, Komarneni Sridhar,Materials Letters 38, 1999, 344.

18. Guo L., Luo H., Gao J , Jianfeng Yang, Materials Letters, 60, 2006, 3011.

19. Sasirekha Natarajan, Rajesh Baskaran, Industrial and Engineering Chemistry Research, 47, 2008, 1868.

20. Stojanovic B.D., Jovalekic C, Vukotic V., Simoes A.Z., Varela J.A, Ferroelectrics, 319 , 2005, 65.

21. Xue Junmin, Wang John, and Wan Dongmei, Journal of American Ceramics Society, 83, 2000, 232.

22. Luo Shaohua, Tang Zilong, Yao Weihua and Zhang Zhongtai, Journal of Microelectronic Engineering, 66, 2003, 147.

23. Won H.I.,. Nersisyan H.H and Won C.W., Materials Letters, 61, 2007, 1492.

24. Anuradha T.V., Ranganathan S., Mimani Tanu and Patil K.C, Scripta Materialia, 44, 2001, 2237.

25. Gorokhovsky A.V., Escalante-Garcia J.I., Sa´nches-Monjara´s T., Vargas-Gutierrez G., Materials Letters ,58, 2004, 2227.

26. Rørvik Per Martin, Lyngdal Tone, Sæterli Ragnhild, Antonius Helvoort T. J. van, Holmestad Randi, Grande Tor, and Einarsrud Mari-Ann, “Inorganic Chemistry Journal, 47, 2008, 3173.

27. Jeffrey J. Urban, Wan Soo Yun, Qian Gu, and Hongkun Park , Journal of American Chemical Society, 124, 2002, 1186.

28. Miao Jing, Hu Chenguo, Liu Hong , Xiong Yufeng ., Materials Letters, 62, 2008, 235.

29. Mao Yuanbing, Banerjee Sarbajit, and Wong Stanislaus S., Journal of American Chemical Society 125, 2003, 15718.

30. Wang X-H., et al, Journal of Electroceramics, 2010, 07, 170.

31. Ying Kuo-Liang, Hsieh T.-E., Journal of Materials Science and Engineering B, 138, 2007, 241.

32. Polotai Anton, et al, Journal of the American Ceramics Society, 88, 2005, 3008.

33. Shi Jian-Lin, Deguchi Yoichi and Sakabe Yukio, Journal of Materials Science, 40, 2005, 454.

34. Park Y. and Song S.A., Material Science Engineering, 47, 1997, 28.

35. Arlt G., et al, Journal of Applied Physics, 58, 1984, 1619.

36. Begg et al, Journal of the American Ceramic Society, 77, 1994, 3186.

37. Li X. et al, Journal of the American Ceramic Society, 80, 1997, 2844.